Complex-Valued Autoencoders with Coherence Preservation for SAR

Reza Mohammadi Asiyabi[a], Mihai Datcu[a,b], Andrei Anghel[a], Holger Nies[c]
[a] Research Center for Spatial Information (CEOSpaceTech), University Politehnica of Bucharest, Bucharest, Romania
[b] Earth Observation Center (EOC), German Aerospace Center (DLR), Wessling, Germany
[c] Center for Sensor Systems (ZESS), University of Siegen, 57074 Siegen, Germany

Abstract

Deep learning techniques have attracted many interests in various fields, including Synthetic Aperture Radar (SAR). A few researches have extended the deep learning framework into the complex-domain to exploit the phase and amplitude of the Complex-Valued (CV)-SAR data. In this study, a complex-valued Convolutional AutoEncoder (CV-CAE) is developed for CV-SAR data reconstruction from the lower resolution azimuth subaperture images. Finally, the performance of the CV-CAE is evaluated, in terms of the reconstruction quality and the coherency preservation, and showed that the CV-CAE is capable of reconstructing the CV-SAR images and preserving the coherency, with a remarkably small training dataset.

1 Introduction

The very large amount of data availability has shifted the data processing paradigm into data intensive methods, especially machine learning algorithms. Deep learning models are proved to be an extremely powerful and versatile methods for many different pattern recognition applications, including image classification and clustering [1], object detection [2], and natural language processing [3]. Following the breakthrough of deep learning methods in the computer vision, remote sensing and Earth Observation scientists grow an enormous interest in this field and have achieved state-of-the-art results by applying deep learning techniques for remote sensing applications.

In the recent studies for instance, Zhang et al. [4] used Convolutional Neural Network (CNN) for classification of 10 urban tree species with both simple and complex backgrounds in RGB optical images, acquired by Unmanned Aerial Vehicles (UAVs). Valero et al. [5] employed Variational AutoEncoders (V-AE) on multispectral Sentinel-2 images to produce a low dimensional image representation and classification. Campos-Taberner et al. [1] proposed to use the relevance of predictors in the classification process to improve the understanding of the behaviour of Recurrent Neural Networks (RNN) in land cover classification with Sentinel-2 data. In another work, Peterson et al. [6] used Landsat-8/Sentinel-2 virtual constellation in deep learning model for the estimation of various water quality measures, including blue-green algae, chlorophyll-α, and turbidity. Debella-Gilo and Gjertsen [7] used Sentinel-2 data with missing information for crop type mapping and evaluated the performances and characteristics of various deep learning models, including CNN and RNN.

In parallel to the huge success of deep learning models in optical remote sensing, many researchers have evaluated the performance of these models with Synthetic Aperture Radar (SAR) images [8]. Most of these attempts directly applied real-valued deep models only to the amplitude of the SAR data, and completely neglected the phase information [9]. However, the phase component of SAR data is a unique information source that should be considered for various information retrieval tasks in SAR data processing. Since most of the developed deep models are designed for real-valued data, Complex-Valued (CV) models have to be developed to exploit both the amplitude and the phase components of the CV-SAR data.

A number of studies have been carried out in this field in the recent years. Akira Hirose is definitely one of the pioneers in CV deep models [10]–[12]. In one of his recent studies, Konishi et al. [13] utilized a complex-valued reservoir computing (CVRC) deep model for Interferometric SAR (InSAR) data classification. The proposed CVRC method increased the classification accuracy and remarkably decreased the computational time. Moreover, Sunaga et al. [14] proposed a complex absolute-value max pooling method to extract complex-amplitude feature patterns for landform classification in InSAR data.

In addition, several other researchers developed CV deep learning models for SAR data processing. Zhang et al. [9] proposed a CV-CNN for SAR data interpretation and compared the results with the real-valued CNN. Shang et al. [15] extended the encoding and decoding paradigm into the complex domain by CV-Convolutional AutoEncoder (CV-CAE), and utilized it for PolSAR data classification. Furthermore, Xie et al. [16] proposed to stack a CV Wishart autoencoder and a CV-AE, in order to develop a Complex-Valued Wishart Stacked AutoEncoder (CV-WSAE) classification model for POLSAR data interpretation.

Phase information in CV-SAR data is a unique component with a sensitive structure, and the phase preservation in SAR data processing should be considered, especially for InSAR applications. Very important characteristics of the SAR system and the physical properties of the target can be extracted from the complex correlation coefficient (Coherency) of the CV-SAR images [17]. The coherency is the most important observation for many InSAR applications, including Digital Elevation Model (DEM) extraction [17].

In this study, we have proposed a CV-CAE to reconstruct CV-SAR images from lower resolution Azimuth subaperture images and the coherency images between them, and evaluated the coherency preservation during the process.
In the second section of this article, the brief theoretical background of the azimuth subaperture in SAR image processing, as well as the transformation of the real-valued AE into the complex domain are provided. In section three, the details of the dataset, as well as the applied experiments and the obtained results are explained. Finally, section four summarizes and concludes the findings of the study.

2 Theoretical Background

In this section, a brief introduction of the azimuth subaperture decomposition and the coherence images calculation are provided. Later, the development of the CV-CAE from real-valued operators is explained.

2.1 Azimuth Subaperture

An advanced signal processing technology is applied to the SAR systems to replace the real aperture antenna with a larger synthetic aperture to achieve a higher azimuth resolution. In the synthetic aperture technology, a target is illuminated from different angles along the flight path of the platform and all the backscattered signals in different azimuth angles are integrated to obtain the higher azimuth resolution. Azimuth subaperture decomposition technique provides the opportunity to obtain images of the targets observed by different azimuth angles in the SAR footprint (i.e., front and back look) [18].
Theoretically, subaperture images should be derived from raw data [18]. However, raw data for many spaceborne SAR sensors are not available, but the pre-processing, applied by the space agencies, preserve the phase information to a reasonable extent [18]. Only the windowing effect which has been applied to reduce the sidelobs, has to be compensated.
Fourier Transform can be used to derive the subaperture images from pre-processed SAR data. Therefore, Fourier Transform converts the original CV-SAR image into its corresponding spectrum in the Fourier frequency domain. Later, the effect of the Hamming window, that has been applied to the original data to reduce the sidelobs, is compensated to achieve a uniform spectrum. The coefficients of the applied Hamming window can be found in the products' documentary, provided by the space agency. Three overlapping new Hamming windows with equal sizes, covering different portions of the spectrum in the azimuth direction, are multiplied by the uniform spectrum to achieve three subaperture spectrums. Finally, Inverse Fourier Transform is used to obtain the azimuth subaperture images. It should be noted that the obtained subaperture images are also in the complex domain.
While using the azimuth subaperture decomposition, one should consider that the subaperture images will have proportionally lower resolution, as we are using only a portion of the full available system bandwidth [18]. Consequently, overlapping subaperture spectrums are used to extent the subaperture range and obtain the higher resolution. In addition, Zero Doppler for the moving targets, including trains or cars, might be in different positions which increases the possibility of defocused targets and miss detection [18].
After obtaining the subaperture images from different polarization channels of the original SAR image, in the next step, a coherence, as illustrated in Equation 1, is computed between different pairs of the subaperture images [18]. In the Equation 1, $C()$ is the coherence between any pair of the subaperture images, Z represents the subaperture images, and $E()$ and $*$ are the expected value over an arbitrary weight window, and respectively, the complex conjugation operator. An 11×11 window with equal weights, ones, is applied in this study.

$$C(Z_1, Z_2) = \frac{E(Z_1 Z_2{}^*)}{\sqrt{E(Z_1 Z_1{}^*)E(Z_2 Z_2{}^*)}} \qquad (1)$$

Figure 1 shows a few examples of the coherence images from the same geographical area. It can be observed that different coherence images emphasized different targets and can be utilized for exploring the diversity of the backscattering signature in subaperture images. Red circles show some objects appeared and emphasized only in one coherence image.

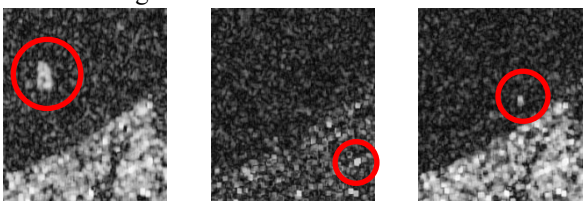

(a) (b) (c)

Figure 1 Different coherency images from the same area, showing different latent information and indicates the ability of the coherency images between different pairs of subapertures for exploring the diversity of backscattering signatures.

2.2 Complex-Valued Convolutional Auto-Encoder (CV-CAE)

In this study, encoding framework is used to represent the CV-SAR images from the lower resolution azimuth subaperture images and the coherency images between them, in a lower dimension latent space, and the decoding framework is used to reconstruct the CV-SAR images. In order to exploit not only the amplitude, but also the phase information in the CV-SAR images, the AE paradigm is extended into the complex domain. In this model, all the layers including convolutional, pooling, batch normalization, and fully connected layers are in complex domain. In addition, the weights and biases in the neurons, and the activation functions are complex-valued. Furthermore, a complex-valued backpropagation, based on the stochastic gradient descent, is used for training the CV-CAE. However, the loss function remains in the real-domain to minimize the empirical issues [19].

2.2.1 Mathematical background

Convolution is an important operator in different CNN models, which extracts the discriminant latent features from the input data. In the complex domain, the output of the convolution, $y_i^{(l+1)} \in \mathbb{C}^{W_2 \times H_2 \times l}$, is computed by the convolution between the input feature map from the previous layer, $X_{iC}^{l} \in \mathbb{C}^{W_1 \times H_1 \times C}$, and the weights of the neurons, $w_{iC}^{(l+1)} \in \mathbb{C}^{F \times F \times C \times l}$, and then adding a bias $b_i^{(l+1)} \in \mathbb{C}^{l}$, as shown in the Equation (2).

$$\begin{aligned} y_i^{(l+1)} &= \sum_{C=1}^{C} w_{iC}^{(l+1)} * X_k^l + b_i^{(l+1)} \\ &= \sum_{C=1}^{C} (\Re(w_{iC}^{(l+1)}) . \Re(X_{iC}^{l}) - \Im(w_{iC}^{(l+1)}) . \Im(X_{iC}^{l})) \\ &\quad + j \sum_{C=1}^{C} (\Re(w_{iC}^{(l+1)}) . \Im(X_{iC}^{l}) - \Im(w_{iC}^{(l+1)}) . \Re(X_{iC}^{l})) \\ &\quad + b_i^{(l+1)} \end{aligned} \quad (2)$$

Where $\mathbb{C}$, $\Re$, and $\Im$ denote the complex domain, real, and imaginary components, respectively. l is the layer number, C is the number of the channels, and the character $*$ denotes the convolution operation [15], [19]. Later, the feature output map of the layer is computed by applying a complex-valued activation function, Rectified Linear Unit (ReLU) in this study, as demonstrated in equation (3).

$$Y_{iC}^{l} = ReLU\left(\Re\left(y_{iC}^{l}\right)\right) + j\, ReLU\left(\Im\left(y_{iC}^{l}\right)\right) \quad (3)$$

Pooling layer in deep learning models, reduce the size of the input image by reducing the redundant information. Max-pooling and Mean-pooling are the most frequently used pooling operators in deep models. In the complex-domain, max-pooling cannot be directly defined [15], and as a result, mean-pooling has been employed in this study. Up-pooling and deconvolution operations, which are used in the decoder framework to reconstruct the image, also can be defined in the same manner [9], [15].

In order to training the CV-CAE, a complex-valued extension of the backpropagation algorithm should be derived. For this purpose, the loss function, $J(\theta)$, of the reconstruction process can be defined as equation (4), where θ represents the trainable parameters, weights and biases, of the model.

$$\begin{aligned} J(\theta) = \frac{1}{2N} \sum_{i=1}^{N} \Big[&\left\| \Re\left(Y_{iC}^{l}\right) - \Re\left(X_{iC}^{l}\right) \right\|^2 \\ &+ \left\| \Im\left(Y_{iC}^{l}\right) - \Im\left(X_{iC}^{l}\right) \right\|^2 \Big] \end{aligned} \quad (4)$$

The weights and the biases of the network can be updated iteratively, using the equations (5), and (6), respectively [9], [15].

$$W_{iC}^{l} = w_{iC}^{l} - \eta \frac{\partial J(\theta)}{\partial w_{iC}^{l}} \quad (5)$$

$$B_{C}^{l} = b_{C}^{l} - \eta \frac{\partial J(\theta)}{\partial b_{C}^{l}} \quad (6)$$

In order to solve the equations (5) and (6), the chain role should be extended to the complex domain to calculate the derivatives of the loss function, $J(\theta)$, with respect to the weights and biases of the model. For instance, this extension is shown in equation (7) for the weight parameters.

$$\begin{aligned} \frac{\partial J(\theta)}{\partial w_{iC}^{l}} &= \frac{\partial J(\theta)}{\partial \Re(w_{iC}^{l})} + \frac{\partial J(\theta)}{\partial \Im(w_{iC}^{l})} \\ &= \left(\frac{\partial J(\theta)}{\partial \Re(Y_{iC}^{l})} \frac{\partial \Re(Y_{iC}^{l})}{\partial \Re(w_{iC}^{l})} + \frac{\partial J(\theta)}{\partial \Im(Y_{iC}^{l})} \frac{\partial \Im(Y_{iC}^{l})}{\partial \Re(w_{iC}^{l})} \right) \\ &\quad + j \left(\frac{\partial J(\theta)}{\partial \Re(Y_{iC}^{l})} \frac{\partial \Re(Y_{iC}^{l})}{\partial \Im(w_{iC}^{l})} + \frac{\partial J(\theta)}{\partial \Im(Y_{iC}^{l})} \frac{\partial \Im(Y_{iC}^{l})}{\partial \Im(w_{iC}^{l})} \right) \end{aligned} \quad (7)$$

2.2.2 Architecture of the CV-CAE

Most popular Python libraries for developing deep neural networks, such as Pytorch and Tensorflow, do not completely support the development of complex-valued deep models, which causes several implementation restrictions and limit the applicability of these models for various applications [19]. As a result, in this study, the real-valued operators, defined in the Pytorch library, are used to develop a series of complex-valued operators, based on the extensions from section 2.2.1, including but not limited to the complex-valued convolution, mean-pooling, ReLU, and Backpropagation algorithm. The developed operators are utilized to define the CV-CAE.

Figure 2 illustrates the architecture of the CV-CAE, as well as the architectures of the inner layers in the model. CV-CAE consists of one input layer, and four down-sampling layers in the encoding section (Red section in **Figure 2**), and four up-sampling, and one output layers in the decoding section (Green section in **Figure 2**). In the architecture of the CV-CAE a complex-valued processing module, consisting of two layers of 2D convolutions, followed by 2D batch normalization layers with ReLU activation functions (will be called "Double-convolution" module in this article) is defined and utilized to build the model.

The Double-convolution module is used as the input layer to feed the data into the model. Later, four down-sampling layers, consisting of a complex-valued mean-pooling layer and a Double-convolution module, are used to encode the input data and extract the latent features. Similarly, in the decoding section, four up-sampling layers, consisting of a complex-valued up-pooling layer and a Double-convolution module, are used. Finally, one complex-valued convolutional layer is used in the output layer.

3 Experimental Results

Sentinel-1 is the SAR imagery mission of the Copernicus programme, which measures the Earth surface in C-band frequency and up to 5 m × 5 m spatial resolution, based on the operation mode [20]. Sentinel-1 mission provides free of charge SAR data in dual-polarization with 6-days revisit time with the constellation of two similar satellites (Sentinel-1A and Sentinel-1B). Three Scenes acquired over Chicago and Houston in the Uniate States, and Sao Paulo in Brazil, in StripMap (SM) mode, are used in this study. **Table 1** summarizes the specifications of these scenes.

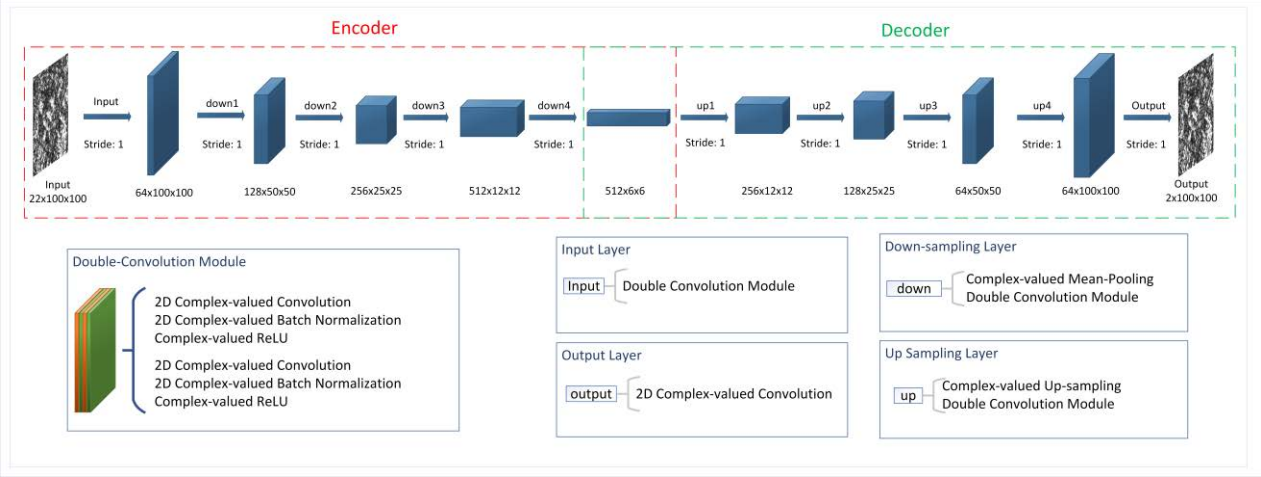

Figure 2 Architecture of the developed CV-CAE, including the architecture of the Double-convolution module, Input, Down-sampling, Up-sampling, and Output layers.

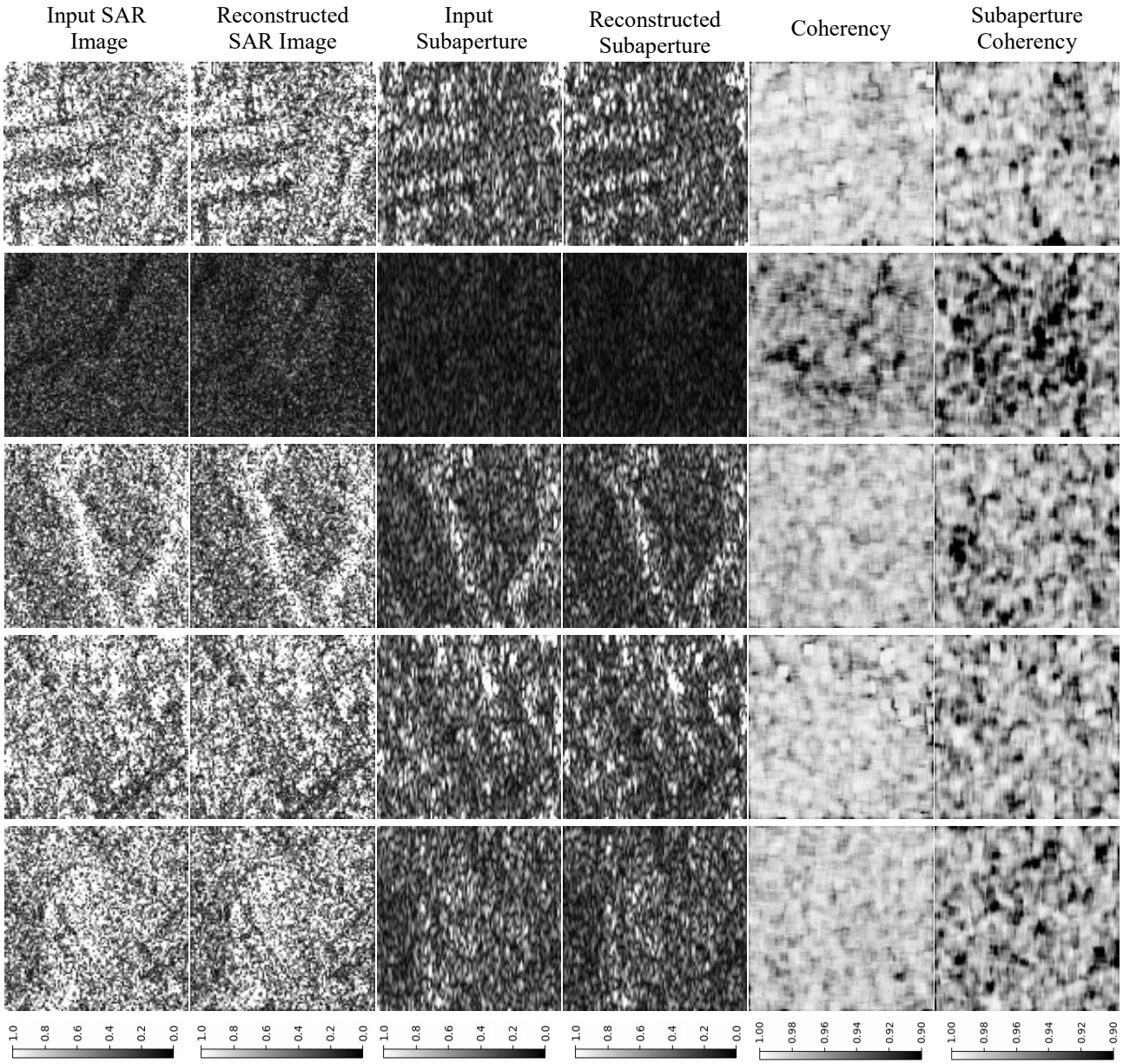

Figure 3 HH polarization of the input and the reconstructed SAR example patches with one example azimuth subaperture of the input and the reconstructed patches, and the coherency image between the SAR and the subaperture images. The coherency is very close to 1 and the intensity range of the image is limited to 0.90-1 for better visualization.

Table 1 Specifications of the Sentinel-1 SAR data, used in this study

Feature	Chicago Scene	Houston Scene	Sao Paulo Scene
Product ID	S1A_S1_SLC__1SDH_20210518T121201_037942_047A61_DE5A	S1B_S3_SLC__1SDH_20210505T001823_026762_033263_16AD	S1A_S3_SLC__1SDH_20210516T213615_037918_0479A0_E1C4
Acquisition Date	2021/05/18	2021/05/05	2021/05/16
Orbit Pass	Descending	Ascending	Ascending
Mission	Sentinel-1A	Sentinel-1B	Sentinel-1A
Acquisition Mode	SM	SM	SM
Product	Level-1 SLC	Level-1 SLC	Level-1 SLC
Polarization	HH, HV	HH, HV	HH, HV
Subset size (pixels)	54900 ×21000	46600×18800	46700×18600

SM = StripMap, SLC = Single Look Complex

The SAR scenes are divided into 100×100-pixel patches. 9000 patches (3000 from each scene) are randomly selected from the dataset and used to train the CV-CAE in this study. The model has been trained with 15 epochs, 10 batch size, and 0.001 learning rate. Later, in order to evaluate the performance of the CV-CAE, in terms of the CV-SAR image reconstruction and phase preservation, several random patches are selected and tested in the trained CV-CAE. The coherency between the input and the reconstructed CV-SAR images are computed. The coherency images are used as the measure of the quality of the reconstructed CV-SAR image, in terms of the preservation of the phase component, as well as modelling the amplitude.

Figure 3 shows some examples of the HH polarization input and the reconstructed patches, along with the azimuth subaperture from the input and the reconstructed patches, and the coherency between the SAR and between the subaperture images. In this figure, the coherency is very close to 1 and as a result, the intensity range of the image is limited to 0.90-1 for better visualization (notice the colour bars). Remarkably high coherency between the input and the reconstructed images as well as the subaperture images indicate that the CV-CAE learned the CV data model and preserved the complex correlation coefficient of the CV-SAR images.

Moreover, **Figure 4** demonstrates the average histogram of the coherency between the input and reconstructed images for 1000 random samples. Since there is no coherency value lower than 0.5, the horizontal axis in **Figure 4** is limited to 0.5-1, for better visualization. Besides, the frequency of the coherency one is about 4000, but the vertical axis is limited to below 1000 for better visualization. This histogram shows that the coherency is very high (close to one in most of the scene) and indicates the preservation of the phase in the CV-SAR image processing.

Concerning the computational efficiency, processing CV-SAR images in the complex-domain is costlier and requires more computational power, because of the complex-valued operators and more parameters to be solved. However, the additional information in the complex-valued data has empowered the deep model to be trained with much smaller training dataset. As mentioned earlier, only 9000 CV-SAR patches have been used in the training stage of the CV-CAE, which is remarkably lower than the frequently used training datasets in real-valued deep models (Usually more than 100,000 patches). Consequently, even though processing one complex-valued patch is more computationally expensive, but the model can be trained with much smaller training dataset, which increases the computational efficiency of the model.

Furthermore, the ability of the complex-valued deep models to be trained with relatively small training datasets will help with the problem of the annotated Ground Truth (GT) data in remote sensing, especially SAR data processing. Generally deep models require a very large annotated dataset for training (Usually more than 100,000 patches), however, collecting GT annotated dataset for training the deep models in earth observation is a big challenge that has limited the applicability of these models in many different applications. In this study, we have showed that the Complex-valued deep models exploit more information from data and are able to train with a smaller training dataset.

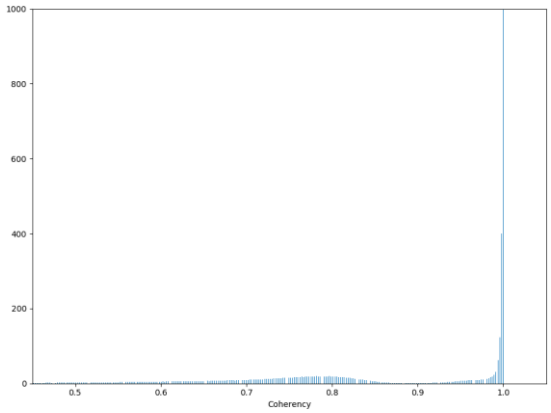

Figure 4 Average histogram of the coherency between the input and the reconstructed images for 1000 random samples.

4 Conclusion

In this study, necessary operators for deep learning models, are extended into the complex domain and utilized to develop a CV-CAE framework for CV-SAR data reconstruction with the azimuth subaperture images and the coherency images between them. All of the operators and the parameters, including the weights and biases, convolutional, batch normalization, down-pooling and up-pooling layers, activation functions, and the Backpropagation algorithm, have been applied in the complex-domain. Finally, the coherency between the input and the reconstructed CV-SAR and the subaperture images are computed and used for evaluation. The high coherency indicated the high quality reconstruction and preserving the phase information of the CV-SAR images. Phase component has a very sensitive structure and special measures should be applied to preserve the structure of the phase information in CV-SAR data processing.

In addition to the high quality reconstruction and coherency preservation, the developed CV-CAE model is trained with only 9000 samples, which is remarkably lower than the frequently used deep models. The capability of being trained with a relatively small dataset indicates the importance of the phase information. Specifically, including the phase information in the training procedure of the deep model has enabled the model to extract the necessary information and train with lower number of the samples.

The promising performance of the developed CV-CAE demonstrated the potential of the CV deep models for various CV-SAR processing applications. In the future studies, the authors suggest to utilize the coherency preserving CV-CAE for latent feature extraction form CV-SAR images, as well as the development of CV deep classification models. Moreover, further inspections should be done on the developed complex-valued deep model, including the comparison with the equivalent real-valued deep models in terms of the information extraction and computational cost, effect of the larger training dataset, and overfitting.

5 Acknowledgement

This project has received funding from the European Union's Horizon 2020 research and innovation programme under the Marie Skłodowska-Curie grant agreement No 860370.

6 Literature

[1] M. Campos-Taberner *et al.*, "Understanding deep learning in land use classification based on Sentinel-2 time series," *Sci. Rep.*, vol. 10, no. 1, pp. 1–12, 2020.

[2] Z.-Q. Zhao, P. Zheng, S. Xu, and X. Wu, "Object detection with deep learning: A review," *IEEE Trans. neural networks Learn. Syst.*, vol. 30, no. 11, pp. 3212–3232, 2019.

[3] L. Deng and Y. Liu, *Deep learning in natural language processing*. Springer, 2018.

[4] C. Zhang, K. Xia, H. Feng, Y. Yang, and X. Du, "Tree species classification using deep learning and RGB optical images obtained by an unmanned aerial vehicle," *J. For. Res.*, vol. 32, no. 5, pp. 1879–1888, 2021.

[5] S. Valero, F. Agulló, and J. Inglada, "Unsupervised Learning of Low Dimensional Satellite Image Representations via Variational Autoencoders," in *2021 IEEE International Geoscience and Remote Sensing Symposium IGARSS*, 2021, pp. 2987–2990.

[6] K. T. Peterson, V. Sagan, and J. J. Sloan, "Deep learning-based water quality estimation and anomaly detection using Landsat-8/Sentinel-2 virtual constellation and cloud computing," *GIScience Remote Sens.*, vol. 57, no. 4, pp. 510–525, 2020.

[7] M. Debella-Gilo and A. K. Gjertsen, "Mapping Seasonal Agricultural Land Use Types Using Deep Learning on Sentinel-2 Image Time Series," *Remote Sens.*, vol. 13, no. 2, p. 289, 2021.

[8] X. X. Zhu *et al.*, "Deep learning meets SAR," *arXiv Prepr. arXiv2006.10027*, 2020.

[9] Z. Zhang, H. Wang, F. Xu, and Y.-Q. Jin, "Complex-valued convolutional neural network and its application in polarimetric SAR image classification," *IEEE Trans. Geosci. Remote Sens.*, vol. 55, no. 12, pp. 7177–7188, 2017.

[10] A. Hirose, *Complex-valued neural networks: theories and applications*, vol. 5. World Scientific, 2003.

[11] A. Hirose, *Complex-valued neural networks*, vol. 400. Springer Science & Business Media, 2012.

[12] K. Ichikawa and A. Hirose, "Singular unit restoration in InSAR using complex-valued neural networks in the spectral domain," *IEEE Trans. Geosci. Remote Sens.*, vol. 55, no. 3, pp. 1717–1723, 2016.

[13] B. Konishi, A. Hirose, and R. Natsuaki, "Complex-Valued Reservoir Computing for Interferometric SAR Applications With Low Computational Cost and High Resolution," *IEEE J. Sel. Top. Appl. Earth Obs. Remote Sens.*, vol. 14, pp. 7981–7993, 2021.

[14] Y. Sunaga, R. Natsuaki, and A. Hirose, "Similar land-form discovery: Complex absolute-value max pooling in complex-valued convolutional neural networks in interferometric synthetic aperture radar," in *2020 International Joint Conference on Neural Networks (IJCNN)*, 2020, pp. 1–7.

[15] R. Shang, G. Wang, M. A Okoth, and L. Jiao, "Complex-valued convolutional autoencoder and spatial pixel-squares refinement for polarimetric SAR image classification," *Remote Sens.*, vol. 11, no. 5, p. 522, 2019.

[16] W. Xie, G. Ma, W. Hua, and F. Zhao, "Complex-valued wishart stacked auto-encoder network for polsar image classification," in *IGARSS 2019-2019 IEEE International Geoscience and Remote Sensing Symposium*, 2019, pp. 3193–3196.

[17] C. López-Martínez and E. Pottier, "Coherence estimation in synthetic aperture radar data based on speckle noise modeling," *Appl. Opt.*, vol. 46, no. 4, pp. 544–558, 2007.

[18] A. Marino, M. J. Sanjuan-Ferrer, I. Hajnsek, and K. Ouchi, "Ship detection with spectral analysis of synthetic aperture radar: A comparison of new and well-known algorithms," *Remote Sens.*, vol. 7, no. 5, pp. 5416–5439, 2015.

[19] J. A. Barrachina, C. Ren, C. Morisseau, G. Vieillard, and J.-P. Ovarlez, "Complex-Valued vs. Real-Valued Neural Networks for Classification Perspectives: An Example on Non-Circular Data," *arXiv Prepr. arXiv2009.08340*, 2020.

[20] D. Geudtner, R. Torres, P. Snoeij, M. Davidson, and B. Rommen, "Sentinel-1 system capabilities and applications," in *2014 IEEE Geoscience and Remote Sensing Symposium*, 2014, pp. 1457–1460.